Design a PLL Filter When Only the Zero Resistor and Capacitor Are Adjustable

By Ken Gentile

Introduction

As described in the references, a standard procedure can be used to determine the values of R_0, C_0, and C_P for a second-order loop filter in a phase-locked loop (PLL). It uses open-loop bandwidth (ω_0) and phase margin (ϕ_M) as design parameters, and can be extended to third-order loop filters to determine R_2 and C_2 (Figure 1). The procedure solves for C_P directly and subsequently derives the remaining values.

In some cases, C_P, R_2, and C_2 may be fixed-value components integrated within the PLL, leaving only R_0 and C_0 available for controlling the loop response. This nullifies the aforementioned procedure because C_P cannot be adjusted. This article proposes an alternative procedure that can be used when the value of C_P is fixed, and addresses limitations imposed by the inability to control the value of C_P.

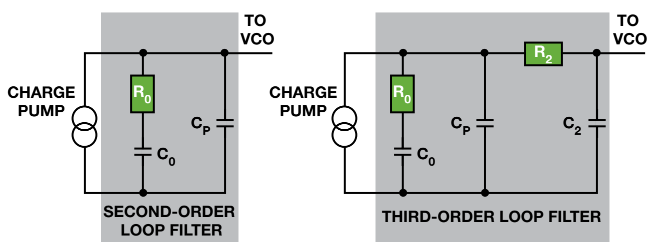

Figure 1. Typical second-order and third-order passive loop filters.

Assumptions

This loop filter design method relies on two assumptions that are typically used in third-order passive filter designs that extend a second-order loop filter design to third-order by compensating for the presence of R_2 and C_2 through adjustment of R_0 and C_0.

1. The pole frequency resulting from R_2 and C_2 should be at least an order of magnitude greater than ω_0 (the desired open-loop unity-gain bandwidth); specifically $f_0 \leq 0.1/(2\pi R_2 C_2)$, where $f_0 = \omega_0/(2\pi)$.
2. The load of the series combination of R_2 and C_2 on the R_0-C_0-C_P network should be negligible.

Transfer Function of a Second-Order Loop Filter

A second-order loop filter has two time constants (T_1 and T_2) associated with its components:

$$T_2 = R_0 C_0 \qquad (1)$$

$$T_1 = \left(\frac{C_P}{C_P + C_0}\right) T_2 \qquad (2)$$

The loop filter's transfer function, in terms of T_1, T_2, and C_P, is important because it plays a significant role in the overall response of the PLL:

$$H_{LF}(s) = \left(\frac{1}{C_P}\right)\left(\frac{T_1}{T_2}\right)\left(\frac{sT_2+1}{s(sT_1+1)}\right) \qquad (3)$$

PLL System Function

The small signal model shown in Figure 2 provides the means for formulating the PLL response and a template for analyzing phase variation at the output resulting from a phase disturbance at the input. Note that the voltage-controlled oscillator (VCO), being a frequency source, behaves like an ideal phase integrator, so its gain (K_V) has a 1/s factor (the Laplace transform equivalent of integration). Hence, the small signal model of a PLL has frequency dependence ($s = \sigma + j\omega$).

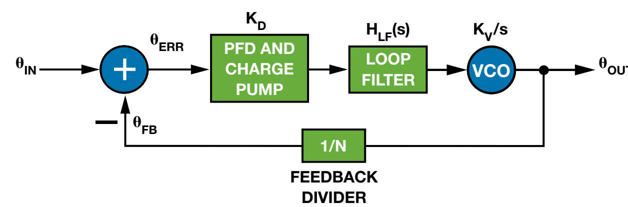

Figure 2. Small signal PLL model.

The closed-loop transfer function (H_{CL}) for a PLL is defined as θ_{OUT}/θ_{IN}. The open-loop transfer function (H_{OL}), defined as θ_{FB}/θ_{IN}, is related to the closed-loop transfer function. It is instructive to express H_{CL} in terms of H_{OL} because the open-loop transfer function contains clues about closed-loop stability:

$$H_{OL}(s) = -K\left(\frac{H_{LF}(s)}{sN}\right) \qquad (4)$$

$$H_{CL}(s) = -N\left(\frac{H_{OL}(s)}{1-H_{OL}(s)}\right) \qquad (5)$$

K represents the combined gains of the phase-frequency detector (PFD), charge pump, and VCO—that is, $K = K_D K_V$, where K_D is the charge pump current in amperes and K_V is the VCO gain in Hz/V. H_{OL}, H_{CL}, and H_{LF} are all functions of s. The negative sign in Equation 4 shows the phase inversion implied by the negative feedback to the summing node in Figure 2. Defining H_{OL} as in Equation 4 leads to subtraction in the denominator of Figure 5, which provides an intuitive explanation of closed-loop stability.

Inspection of Equation 5 reveals a potential loop stability problem. Given that H_{OL} is a function of complex frequency ($s = \sigma + j\omega$), it necessarily has frequency dependent magnitude and phase components. Therefore, if H_{OL} simultaneously exhibits unity gain and zero phase shift (or any integer multiple of 2π radians) for any particular value of s, the denominator of H_{CL} becomes zero, the closed-loop gain becomes undefined, and the system becomes completely unstable. This implies that stability is governed by the frequency-dependent magnitude and phase characteristics of H_{OL}. In fact, at the frequency for which the magnitude of H_{OL} is unity, the phase of H_{OL} must stay far enough from zero (or any integer multiple of 2π) to avoid a zero denominator in Equation 5.

The frequency, ω_0, at which the magnitude of H_{OL} is unity, holds great importance. The phase of H_{OL} at ω_0 defines the phase margin of the system ϕ_M. Both ω_0 and ϕ_M can be derived from H_{OL}.

Defining R_0 and C_0 in Terms of ω_0 and ϕ_M

Using the design parameters ω_0 and ϕ_M to determine the values of R_0 and C_0 requires expressions containing those four variables and other constant terms. Start with Equation 4, because it defines H_{OL}. This includes H_{LF}, which includes R_0 and C_0 via T_1 and T_2. Since H_{OL} has magnitude and phase, it stands to reason that ω_0 and ϕ_M can be incorporated as well.

Substituting Equation 3 into Equation 4 and rearranging terms yields Equation 6, which presents H_{OL} in terms of T_1 and T_2 along with constants K, N, and C_P:

$$H_{OL}(s) = -\left(\frac{K}{s^2 N C_P}\right)\left(\frac{T_1}{T_2}\right)\left(\frac{sT_2+1}{sT_1+1}\right) \qquad (6)$$

Evaluation at s = $j\omega$, yields the frequency response of H_{OL}:

$$H_{OL}(j\omega) = -\left(\frac{K}{(j\omega)^2 N C_P}\right)\left(\frac{T_1}{T_2}\right)\left(\frac{j\omega T_2+1}{j\omega T_1+1}\right) \qquad (7)$$

The $(j\omega)^2$ term in the denominator simplifies to $-\omega^2$:

$$H_{OL}(j\omega) = \left(\frac{K}{\omega^2 N C_P}\right)\left(\frac{T_1}{T_2}\right)\left(\frac{j\omega T_2+1}{j\omega T_1+1}\right) \qquad (8)$$

The magnitude and phase of H_{OL} are:

$$|H_{OL}(j\omega)| = \left(\frac{K}{\omega^2 N C_P}\right)\left(\frac{T_1}{T_2}\right)\left(\frac{1}{1+(\omega T_1)^2}\right)\sqrt{(1+\omega^2 T_1 T_2)^2 + \omega^2 (T_2 - T_1)^2} \qquad (9)$$

$$\angle H_{OL}(j\omega) = arctan(\omega T_2) - arctan(\omega T_1) \qquad (10)$$

Keep in mind that T_1 and T_2 are shorthand expressions for algebraic combinations of R_0, C_0, and C_P. Evaluating Equation 9 at $\omega = \omega_0$ and setting $|H_{OL}| = 1$ defines the unity gain frequency, ω_0, as the frequency at which the magnitude of H_{OL} is unity.

$$1 = \left(\frac{K}{{\omega_0}^2 N C_P}\right)\left(\frac{T_1}{T_2}\right)\left(\frac{1}{1+(\omega_0 T_1)^2}\right)\sqrt{(1+{\omega_0}^2 T_1 T_2)^2 + {\omega_0}^2 (T_2 - T_1)^2} \qquad (11)$$

Similarly, evaluating Equation 10 at $\omega = \omega_0$ and setting $\angle H_{OL} = \phi_M$ defines the phase margin, ϕ_M, as the phase of H_{OL} at frequency ω_0 (the unity gain frequency).

$$\Phi_M = arctan(\omega_0 T_2) - arctan(\omega_0 T_1) \qquad (12)$$

It is a trivial matter to expand Equation 11 and Equation 12 by substituting Equation 1 for T_2 and Equation 2 for T_1, which brings R_0 and C_0 into the equations. Hence, we have succeeded in relating ω_0 and ϕ_M to the variables R_0 and C_0 along with constants K, N, and C_P.

Simultaneously solving the resulting equations for R_0 and C_0 is no trivial task. The symbolic processor available in MathCad® can solve the two simultaneous equations, but arccos must be substituted for arctan. This transformation enables the symbolic processor to solve for R_0 and C_0, yielding the following solution sets (R_{0A}, C_{0A}; R_{0B}, C_{0B}; R_{0C}, C_{0C}; and R_{0D}, C_{0D}). See the Appendix for details on transforming Equation 12 to use the arccos function.

$$R_{0A} = \frac{\omega_0 K N\sqrt{1-\cos^2(\Phi_M)}}{K^2 + 2KC_P N{\omega_0}^2\cos(\Phi_M) + (C_P N{\omega_0}^2)^2} \qquad C_{0A} = -\left(\frac{K^2 + 2KC_P N{\omega_0}^2\cos(\Phi_M) + \left(C_P N{\omega_0}^2\right)^2}{N{\omega_0}^2(C_P N{\omega_0}^2 + K\cos(\Phi_M))}\right)$$

$$R_{0B} = -\left(\frac{\omega_0 K N\sqrt{1-\cos^2(\Phi_M)}}{K^2 + 2KC_P N{\omega_0}^2\cos(\Phi_M) + (C_P N{\omega_0}^2)^2}\right) \qquad C_{0B} = -\left(\frac{K^2 + 2KC_P N{\omega_0}^2\cos(\Phi_M) + \left(C_P N{\omega_0}^2\right)^2}{N{\omega_0}^2(C_P N{\omega_0}^2 + K\cos(\Phi_M))}\right)$$

$$R_{0C} = \frac{\omega_0 K N\sqrt{1-\cos^2(\Phi_M)}}{K^2 - 2KC_P N{\omega_0}^2\cos(\Phi_M) + (C_P N{\omega_0}^2)^2} \qquad C_{0C} = -\left(\frac{K^2 - 2KC_P N{\omega_0}^2\cos(\Phi_M) + \left(C_P N{\omega_0}^2\right)^2}{N{\omega_0}^2(C_P N{\omega_0}^2 - K\cos(\Phi_M))}\right)$$

$$R_{0D} = -\left(\frac{\omega_0 K N\sqrt{1-\cos^2(\Phi_M)}}{K^2 - 2KC_P N{\omega_0}^2\cos(\Phi_M) + (C_P N{\omega_0}^2)^2}\right) \qquad C_{0D} = -\left(\frac{K^2 - 2KC_P N{\omega_0}^2\cos(\Phi_M) + \left(C_P N{\omega_0}^2\right)^2}{N{\omega_0}^2(C_P N{\omega_0}^2 - K\cos(\Phi_M))}\right)$$

This result is problematic because the goal was to solve for R_0 and C_0 given ω_0 and ϕ_M, but this indicates four possible R_0, C_0 pairs instead of a unique R_0, C_0 pair. However, closer inspection of the four results leads to a single solution set as follows.

Note that in the context of modeling a PLL, all of the variables in the above equations possess positive values, including $\cos(\phi_M)$ because ϕ_M is constrained to values between 0 and $\pi/2$. As a result, C_{0A} and R_{0B} are clearly negative quantities. Therefore, solution sets R_{0A}, C_{0A} and R_{0B}, C_{0B} are immediately ruled out because negative component values are not acceptable. The R_{0C}, C_{0C} and R_{0D}, C_{0D} results require further analysis, however.

Note that the four equations involving R_{0C}, C_{0C} and R_{0D}, C_{0D} possess the common factor:

$$K^2 - 2KC_PN\omega_0{}^2\cos(\Phi_M) + (C_PN\omega_0{}^2)^2 \quad (13)$$

Closer inspection reveals that Expression 13 has the form $a^2 - (2ac)\cos(\beta) + c^2$. Equating this with the arbitrary quantity, b^2, yields:

$$b^2 = a^2 + c^2 - (2ac)\cos(\beta) \quad (14)$$

Equation 14, the Law of Cosines, relates a, b, and c as the lengths of the three sides of a triangle with β being the interior angle of the vertex opposite side b. Since b^2 is the square of the length of one side of a triangle, it must be a positive quantity, which implies the right side of Equation 14 must also be positive. Thus, Expression 13 must be a positive quantity, which means the denominator of R_{0D} is positive. The numerator of R_{0D} is also positive, therefore R_{0D} must be negative, which rules out the R_{0D}, C_{0D} solution set. This leaves only the R_{0C}, C_{0C} pair as a contender for the simultaneous solution of Equation 11 and Equation 12.

$$R_0 = \frac{\omega_0 KN\sqrt{1-\cos^2(\Phi_M)}}{K^2 - 2KC_PN\omega_0{}^2\cos(\Phi_M) + (C_PN\omega_0{}^2)^2} \quad (15)$$

$$C_0 = \frac{K^2 - 2KC_PN\omega_0{}^2\cos(\Phi_M) + \left(C_PN\omega_0{}^2\right)^2}{N\omega_0{}^2(K\cos(\Phi_M) - C_PN\omega_0{}^2)} \quad (16)$$

Constraints on R_0 and C_0

Although Equation 15 and Equation 16 are contenders for the simultaneous solution of Equation 11 and Equation 12, they are only valid if they result in positive values for both R_0 and C_0. Close inspection of R_0 shows it to be positive—its numerator is positive, because the range of $\cos^2(x)$ is 0 to 1—and its denominator is the same as Expression 13, which was previously shown to be positive. The numerator of C_0 is also the same as Expression 13, so C_0 is positive as long as its denominator satisfies the following condition:

$$K\cos(\Phi_M) > C_PN\omega_0{}^2 \quad (17)$$

This is depicted graphically in Figure 3, in which the left and right sides of Equation 17 are each equated to y (blue and green curves) with the horizontal axis sharing ω_0 and ϕ_M. The intersection of the two curves marks the boundary condition for ω_0 and ϕ_M. The condition under which Equation 17 is true appears as the red arc. The portion of the horizontal axis beneath the red arc defines the range of ϕ_M and ω_0 that ensures C_0 is positive. Note the point on the horizontal axis directly below the intersection of the blue and green curves establishes ϕ_{M_MAX}, the maximum value of ϕ_M to ensure C_0 is positive.

$$\Phi_{M\_MAX} = \arccos\left(\frac{C_PN\omega_0{}^2}{K}\right) \text{radians} \quad (18)$$

Equation 18 requires that $C_PN\omega_0{}^2$ be less than K in order to satisfy the constraints of the arccos function for ϕ_{M_MAX} between 0 and $\pi/2$. This establishes ω_{0_MAX}, the upper limit on ω_0 to ensure C_0 is positive.

$$\omega_{0\_MAX} = \sqrt{\frac{K}{C_PN}} \text{ radians/s} \quad (19)$$

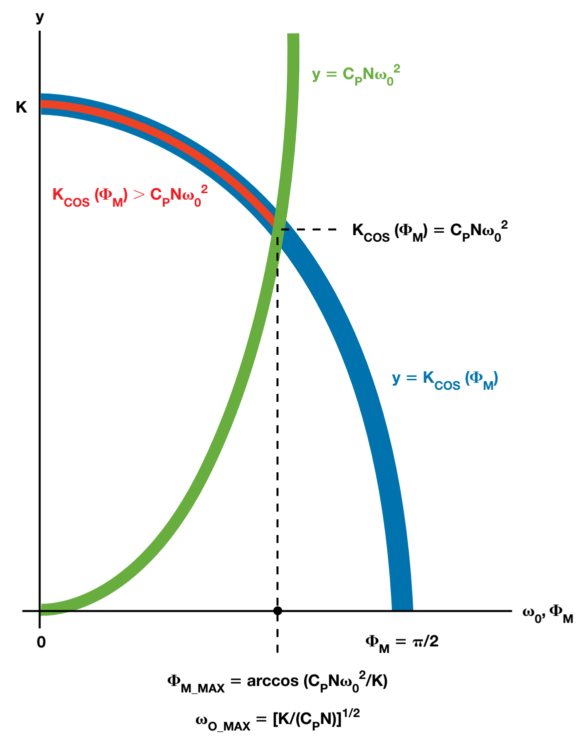

Figure 3. Constraint on C_0 denominator.

Compensating for R_2 and C_2 (Third-Order Loop Filter)

In the case of a third-order loop filter, components R_2 and C_2 introduce additional phase shift, $\Delta\phi$, relative to the second-order loop filter:

$$\Delta\Phi = -\arctan(\omega_0 R_2 C_2) \quad (20)$$

To deal with this excess phase shift, subtract it from the desired value of ϕ_M:

$$\Phi_{M\_MAX} = \Phi_M - \Delta\Phi = \Phi_M + arctan(\omega_0 R_2 C_2) \qquad (21)$$

Applying ϕ_{M_NEW} to Equation 15 and Equation 16 results in different values for R_0 and C_0 than for the second-order solution, with the new values compensating for the excess phase shift introduced by R_2 and C_2. The presence of R_2 and C_2 also affects ϕ_{M_MAX}, the maximum allowable value of ϕ_M. The new maximum value of ϕ_M ($\phi_{M\_MAX\_NEW}$) is

$$\Phi_{M\_MAX\_NEW} = \Phi_{M\_MAX} + \Delta\Phi = arccos(\omega_0^2 N C_P / K) - arctan(\omega_0 R_2 C_2) \qquad (22)$$

Conclusion

This article demonstrates using open-loop unity-gain bandwidth (ω_0) and phase margin (ϕ_M) as design parameters for second-order or third-order loop filters when only components R_0 and C_0 are adjustable. Simulation of a PLL with a second-order loop filter using R_0 and C_0 yields an exact match to the theoretical frequency response of H_{OL} and the resulting phase margin, thereby validating the equations. The parameters ω_0 and ϕ_M have upper bounds for a second-order loop filter per Equation 19 and Equation 18, respectively.

The procedure for determining R_0 and C_0 assumed a second-order loop filter, but is extendible to third-order loop filter designs by adjusting the desired phase margin (ϕ_M) to a new value (ϕ_{M_NEW}) per Equation 21, yielding a new upper bound ($\phi_{M\_MAX\_NEW}$) per Equation 22.

Although simulations using a second-order loop filter validated Equation 15 and Equation 16, validating the equations that extend the design procedure to third-order loop filter designs requires a redefinition of the loop filter response, $H_{LF}(s)$, to include R_2 and C_2 as follows:

$$H_{LF}(s) = \frac{sR_0C_0 + 1}{s(s^2R_0R_2C_0C_2C_P + sR_2C_0C_2 + sR_0C_0C_P + sR_2C_2C_P + sR_0C_0C_2 + C_0 + C_2 + C_P)}$$

The incorporation of this form of H_{LF} into the H_{OL} and H_{CL} equations enables simulations of third-order loop filter designs using R_0 and C_0. Such simulations reveal the calculated values of R_0 and C_0 deviate from the theoretical frequency response and phase margin associated with H_{OL} for a PLL when using a third-order loop filter. This is predominantly due to the effect of R_2 and C_2 on H_{OL} in a third-order loop filter.

Recall that the formulas for R_0 and C_0 assume a second-order loop filter, but R_2 and C_2 do not exist in a second-order filter, so including them as part of the loop filter constitutes a source of error in spite of adjusting R_0 and C_0 to compensate for the phase shift introduced by R_2 and C_2. Even in the presence of this error, however, simulation indicates that using the adjusted values of R_0 and C_0, but limiting the choice of ω_0 to a maximum of ¼ of the value dictated by Equation 19 yields acceptable results. In fact, the simulated open-loop bandwidth and phase margin results deviate only slightly from the design parameters (ω_0 and ϕ_M) for a PLL using a third-order loop filter.

Simulation Results

The following is the result of running four simulations of a PLL with a third-order loop filter. The simulations all have the following fixed-loop filter components and PLL parameters:

C_P = 1.5 nF

R_2 = 165 kΩ

C_2 = 337 pF

K_D = 30 μA

K_V = 3072 (25 ppm/V at 122.88 MHz)

N = 100

Simulation 1 and Simulation 2 use ω_0 = 100 Hz, which is near the calculated upper limit of 124.8 Hz (ω_{0_MAX}). As such, Simulation 1 and Simulation 2 deviate from the design parameter values (ω_0 and ϕ_M) by nearly 10%. On the other hand, Simulation 3 and Simulation 4 use ω_0 = 35 Hz, which is approximately ¼ the upper limit. As expected, Simulation 3 and Simulation 4 hold much closer to the design parameters (ω_0 and ϕ_M), yielding an error of only about 1%.

Table 1 summarizes the simulation results and also includes the calculated values of R_0, C_0, ω_{0_MAX}, and ϕ_{M_MAX} for the given design parameters, ω_0 and ϕ_M. Note that for the purpose of comparison it would be preferable for both Simulation 1 and Simulation 3 to use ϕ_M = 80°, but Simulation 1 must satisfy the constraint imposed by Equation 22 of ϕ_M < 48° (hence the choice of 42°).

Table 1: Simulation Summary

Parameter	Simulation 1		Simulation 2		Simulation 3		Simulation 4	
	ω_0	ϕ_M	ω_0	ϕ_M	ω_0	ϕ_M	ω_0	ϕ_M
Design	100 Hz	42°	100 Hz	30°	35 Hz	80°	35 Hz	30°
Simulation	93.1 Hz	38.7°	92.5 Hz	27.1°	34.9 Hz	79.0°	34.7 Hz	29.3°
R_0	969.6k kΩ		1118 kΩ		240.1 kΩ		139.9 kΩ	
C_0	14.85 nF		3.670 nF		225.5 nF		21.24 nF	
ω_{0_MAX}	124.8 Hz		124.8 Hz		124.8 Hz		124.8 Hz	
ϕ_{M_MAX}	48.0°		48.0°		84.8°		84.8°	

Figure 4 and Figure 5 show the open- and closed-loop response for each simulation.

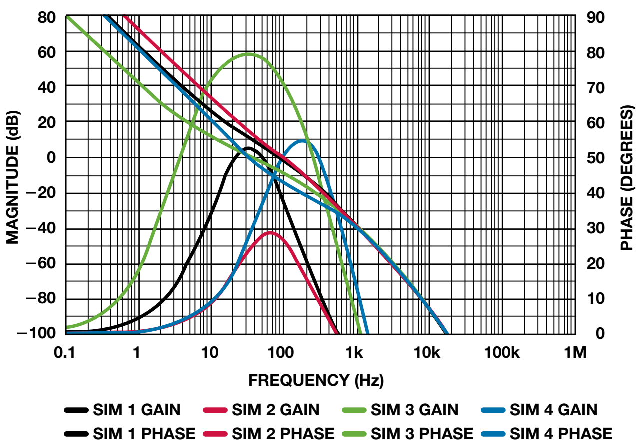

Figure 4. Open-loop gain and phase.

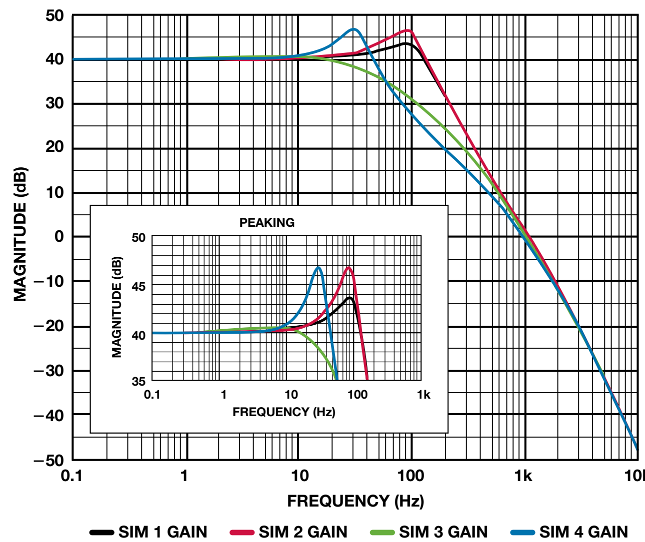

Figure 5. Closed-loop gain.

Appendix—Converting the Discontinuous Arctan Function to the Continuous Arccos Function

Equation 10 demonstrates that the angle ϕ is the difference between angle θ_2 and angle θ_1, where $\theta_2 = \arctan(\omega T_2)$ and $\theta_1 = \arctan(\omega T_1)$. Furthermore, ωT_2 is expressible as x/1 and ωT_1 as y/1:

$$\Phi = \theta_2 - \theta_1 = arctan\left(\frac{x}{1}\right) - arctan\left(\frac{y}{1}\right)$$

This implies the geometric relationship shown in Figure 6, with θ_1 and θ_2 defined by the triangles of Figure 6 (b) and (a), respectively. Figure 6 (c) combines these two triangles to show ϕ as the difference between θ_1 and θ_2.

The Law of Cosines relates an interior angle (θ) of a triangle to the lengths of the three sides of the triangle (a, b, and c) as follows:

$$c^2 = a^2 + b^2 + 2ab\cos(\theta)$$
$$(\theta \text{ is the angle opposite side c})$$

Applying the Law of Cosines to angle ϕ in Figure 6 (c) yields:

$$(x-y)^2 = \left(\sqrt{1+x^2}\right)^2 + \left(\sqrt{1+y^2}\right)^2 - 2\sqrt{1+x^2}\sqrt{1+y^2}\cos\Phi$$

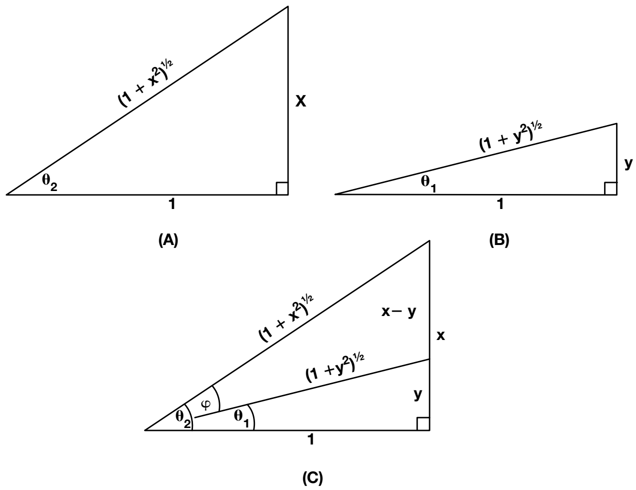

Figure 6. Geometric representation of Equation 10.

Solving for ϕ:

$$\Phi = arccos\left(\frac{1 + xy}{\sqrt{(1 + x^2)(1 + y^2)}}\right)$$

But, $x/1 = \omega T_2$ and $y/1 = \omega T_1$, allowing ϕ to be expressed in terms of T_1 and T_2.

$$\Phi = arccos\left(\frac{1 + \omega^2 T_1 T_2}{\sqrt{[1 + (\omega T_2)^2][1 + (\omega T_1)^2]}}\right)$$

References

Brennan, Paul V. *Phase-Locked Loops: Principles and Practice*. McGraw-Hill, 1996.

Keese, William O. AN-1001, National Semiconductor Application Note, *An Analysis and Performance Evaluation of a Passive Filter Design Technique for Charge Pump Phase-Locked Loops*. May 1996.

MT-086: Fundamentals of Phase Locked Loops (PLLs).

PLLs/PLLs with Integrated VCOs.

Ken Gentile [ken.gentile@analog.com] joined Analog Devices in 1998 as a system design engineer with the Clock and Signal Synthesis product line in Greensboro, NC, where he specializes in direct digital synthesis, analog filter design, and writing GUI-based engineering tools in MATLAB. Ken holds 10 patents. He has published 14 articles in various industry trade journals and over a dozen ADI application notes, as well as having presented at ADI's annual General Technical Conference (GTC) in 2001, 2005, and 2006. He graduated with honors in 1996 with a B.S.E.E. from North Carolina State University. In his spare time, Ken enjoys reading, mathematical puzzles, and most anything related to science, engineering, and "backyard" astronomy.

Ken Gentile

Also by this Author:

Reconstruct a DAC Transfer Function from Its Harmonic Spectral Content

Volume 43, Number 1